Electronic Supplementary Material (ESI) for Materials Chemistry Frontiers.

Non-Covalent Molecular Tweezer/Guest Complexation with Pt(II)···Pt(II) Metal–Metal Interactions: Toward Intelligent Photocatalytic Materials

Zijian Li, Yifei Han, Zongchun Gao, Tengfei Fu, and Feng Wang*

CAS Key Laboratory of Soft Matter Chemistry, iChEM, Department of Polymer Science and Engineering, University of Science and Technology of China, Hefei, Anhui 230026, P. R. China. E-mail: drfwang@ustc.edu.cn.

Supporting Information

1. Materials and methods

9,10-Dimethylanthracene (DMA), copper(I) iodide (CuI), 2,6-diphenylpyridine, 1-(4-ethynyl-2-pyridinyl)-ethanone were reagent grade and used as received. [Pt(C^N^C)(DMSO)], [Pt(tpy)Cl](BF$_4$), compounds **2a**–**b** were synthesized according to the previously reported procedures.[S1–S4] Other reagents and solvents were employed as purchased.

^{1}H NMR spectra was collected on a Varian Unity INOVA-300 spectrometer with TMS as the internal standard. ^{13}C NMR spectra were recorded on a Varian Unity INOVA-300 spectrometer at 75 MHz. Electrospray ionization mass spectra (ESI-MS) were obtained on a Bruker Esquire 3000 plus mass spectrometer (Bruker-Franzen Analytik GmbH Breman, Germany), equipped with an ESI interface and ion trap analyzer. Time-of-flight mass spectra (TOF-MS) were obtained on matrix-assisted laser desorption ionization-time of flight (autoflex speed MALDI/TOF, Bruker). UV/Vis spectra were recorded on a UV-1800 Shimadzu spectrometer. Fluorescent spectra were recorded on a Fluoromax-4 spectrofluorometer. Titration Calorimetry (ITC) experiments were carried out with a Microcal VP-ITC apparatus at 298 K. For DFT calculations, all of the optimized geometries were optimized *via* Gaussian 09 (revision D.01) software package.[S5] Light elements such as C, H, O and N were depicted by 3–21G, whilst the S atoms were described by 6–31G(d) calculation level. Notably, the corresponding Los Alamos core potentials Lanl2dz were deliberately set as basis sets for the heavy Pt^{2+} atoms.

General method for the determination of heterodimeric binding constants via UV-Vis titration measurements: It depends on the UV/Vis intensity changes of MMLCT absorption band upon UV–Vis titration. Briefly, treating the collected absorbance data (*A*) *vs* concentration of the titrating species (C_A) with a non-linear least-squares curve-fitting equation affords the binding constants. For 1 : 1 host/guest complexation, the binding constant is calculated according to the following equation:

$$A = A_0 + \frac{A_{\text{lim}} - A_0}{2C_0}\left[C_0 + C_A + 1/K_S - \left[\left(C_0 + C_A + 1/K_S \right)^2 - 4C_0C_A \right]^{1/2} \right] \quad \textbf{(Eq. S1)}$$

In particular, A_0 and A are the absorbance intensity of the titrated sample at the MMLCT band with and without presence of the titrating species, respectively. [C_0] is the total concentration of the titrated sample, while [C_A] is the concentration of the titrating species. A_{lim} is the limiting value of absorbance in the presence of excess donor and K_S is the binding constant.

*2. Preferential conformation determination for **1b***

Theoretically, molecular tweezer **1b**, together with the counterpart receptor **1a**, could possibility adopt "*U*"- and "*W*"-shaped conformations. To clarify which conformation is more stable, we resorted to the thermotical calculations.[S6] Specifically, the model molecules (**M1a**-*U*, **M1a**-*W*, **M1b**-*U*, and **M1b**-*W*, see Figure S1) were submitted to the DFT calculations. As can be seen, no obvious preference takes place for **M1a**, because of the relatively low energy barrier between "*U*"- and "*W*"-shaped conformations (ΔE = 1.77 kJ/mol). In sharp contrast, **M1b** prefers the "*U*"-shaped conformation, since it is much more stable than the "*W*"-shaped one (ΔE = 71.20 kJ/mol). Such phenomena could be primarily ascribed to the electronic repulsion between nitrogen lone pairs.[S7] Depending on these theoretical studies, it can be concluded that molecular tweezer receptor **1b** also prefers to adopting "*U*"-shaped conformation, with the co-facial conformation for two electron-deficient alkynylplatinum(II) terpyridine pincers.

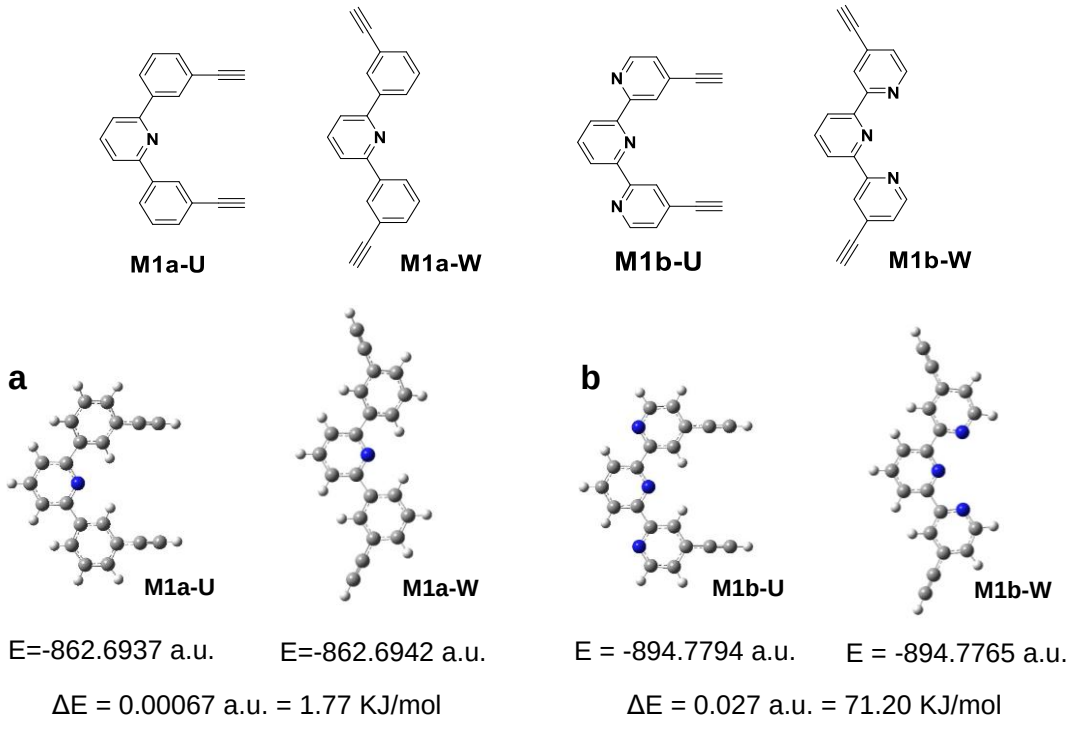

Figure S1. DFT calculations for a) **M1a** and b) **M1b**. All calculations are based on B3LYP/6-31G(d) level.

*3. Photophysical behaviors of **1a** and **1b***

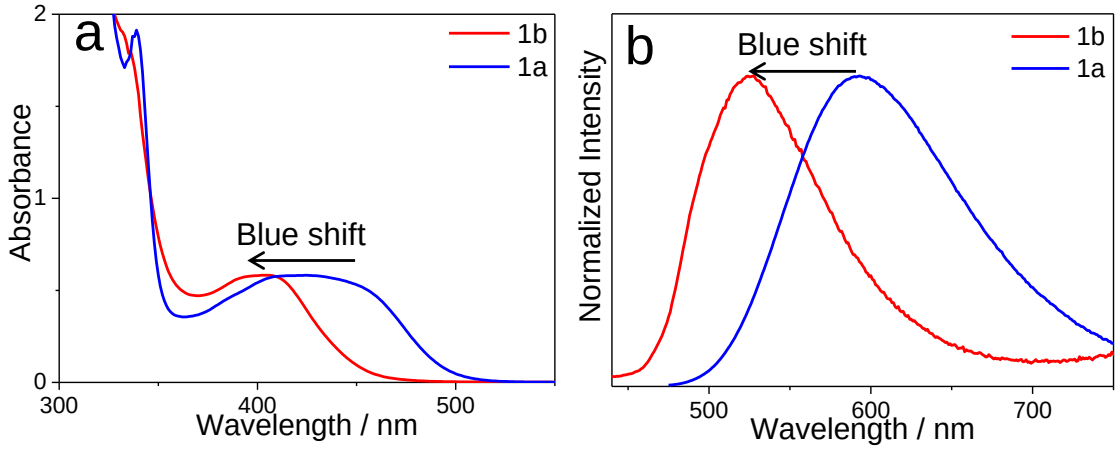

Figure S2. a) UV/Vis and b) fluorescent spectra ($CHCl_3/CH_3CN$ = 1 : 1, 0.05 mM) of molecular tweezers **1a** (blue line) and **1b** (red line). As can be seen, the MLCT/LLCT absorption and emission bands of **1b** are blue-shifted than those of **1a**.

*4. Non-covalent complexation between **1b** and **2a***

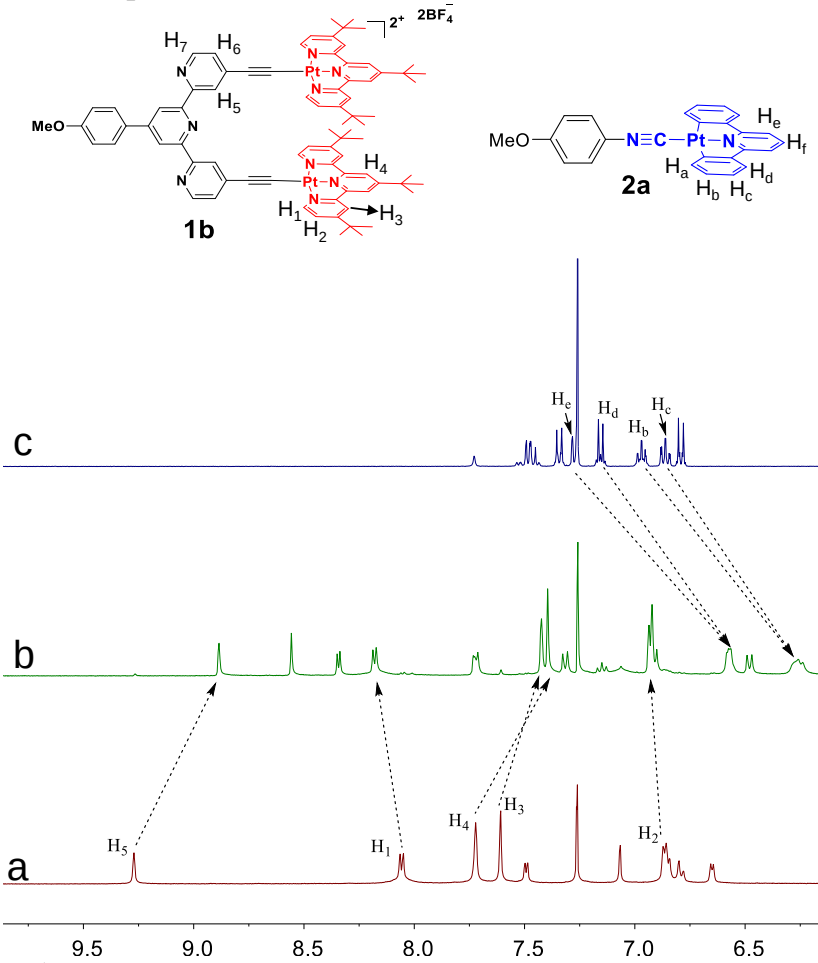

Figure S3. Partial ^{1}H NMR spectra (300 MHz, $CDCl_3/CD_3CN$ = 1 : 1, 298 K, 2.00 mM) of a) **1b**; b) 1 : 1 mixture of **1b** and **2a**; c) **2a**. Upon mixing **1b** and **2a** together, the aromatic terpyridine protons on **1b** and aromatic diphenylpyridine protons on **2a** undergo obvious upfield shifts (–0.22, –0.30, –0.58 and –0.71 ppm for H_3, H_4, H_d and H_e, respectively). Hence, electron donor–acceptor interactions exist between electron-deficient terpyridine pincers on **1b** and electron-rich diphenylpyridine unit on **2a**.

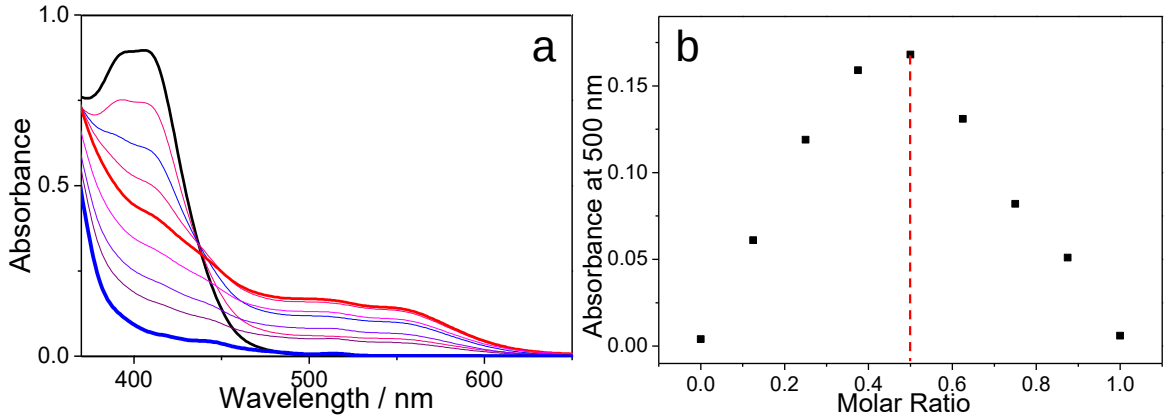

Figure S4. a) UV/Vis spectra for the mixture of **1b** and **2a**, by keeping the total concentration constant ($CHCl_3/CH_3CN$ = 1 : 1, [**1b**] + [**2a**] = 0.10 mM). b) Job's plot. The curve shows 1 : 1 binding stoichiometry between **1b** and **2a**, by plotting the absorbance at 500 nm against the mole fraction of guest **2a**.

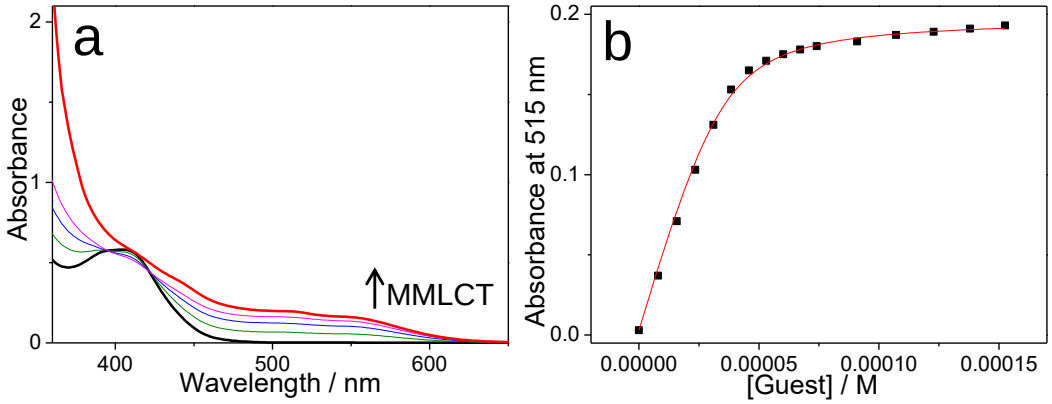

Figure S5. a) UV/Vis spectral changes of **1b** (0.05 mM, $CHCl_3$: CH_3CN = 1 : 1) upon gradual addition of **2a**. b) Intensity changes of absorbance at 515 nm. The MMLCT band of **1b**, predominately locating on the region of approximately 450–600 nm, undergoes gradual increase for the absorption intensity upon progressive addition of **2a**. Nonlinear curve-fitting of the collected absorbance data at 515 nm provides the K_a value of (2.53 ± 0.29) × 10^5 M^{-1}.

*5. Non-covalent complexation between **1b** and **2b***

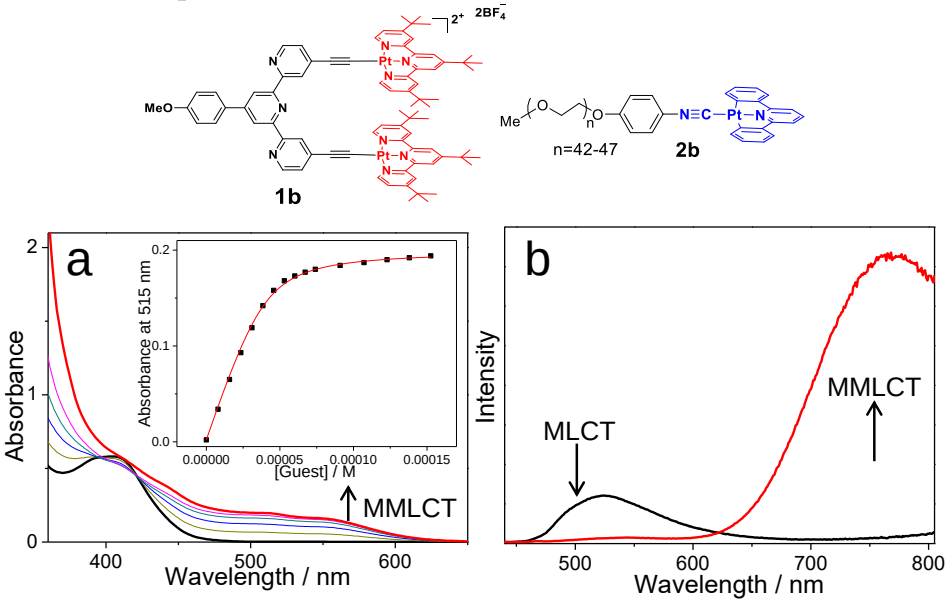

Figure S6. a) UV/Vis absorption spectral changes of **1b** (0.05 mM, $CHCl_3$: CH_3CN = 1 : 1) upon gradual addition of **2b**. Inset: intensity changes of absorbance at 515 nm. b) Fluorescent spectra (0.05 mM, $CHCl_3$: CH_3CN = 1 : 1) of **1b** (black line) and **1b**/**2b** (red line). The emergence of MMLCT absorption/emission bands support the presence of Pt---Pt metal–metal interactions for complex **1b**/**2b**. Nonlinear curve-fitting of the collected absorbance data at 515 nm provides the K_a value of (2.30 ± 0.22) × 10^5 M^{-1} for complex **1b**/**2b**.

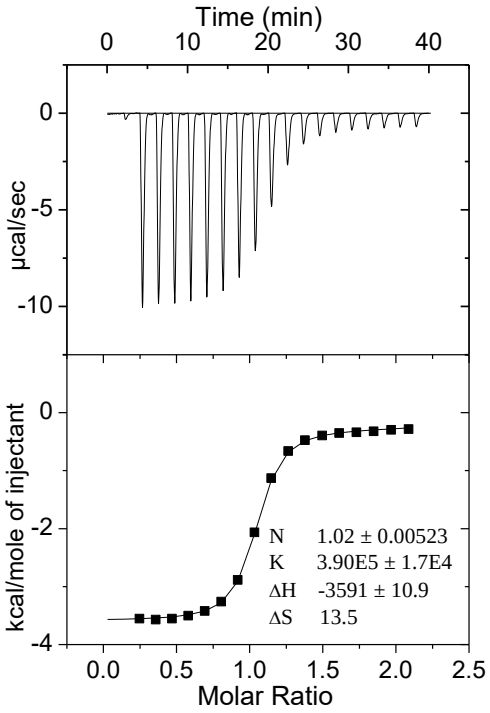

Figure S7. ITC experiments by consecutive injecting of **2b** (8.00 mM) into the solution of **1b** (0.40 mM, $CHCl_3$: CH_3CN = 1 : 1). The binding stoichiometry between **1b** and **2b** is determined to be 1 : 1, as reflected by the abrupt change in the curve. Fitting the exothermic binding isotherm data with one-site model provides the K_a value of (3.90 ± 0.17) × 10^5 M^{-1} for **1b**/**2b**. Such results are highly consistent with those of the UV/Vis titration experiments (Figure S6a).

*6. Non-covalent complexation between **1a** and **2a***

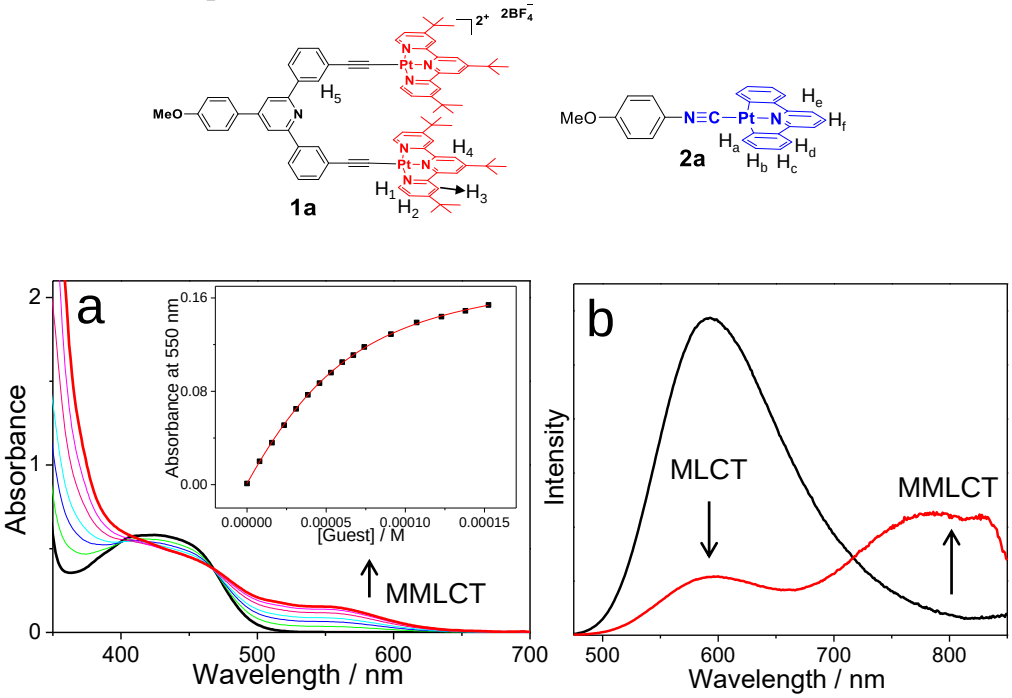

Figure S8. a) UV/Vis absorption spectral changes of **1a** (0.05 mM, $CHCl_3$: CH_3CN = 1 : 1) upon gradual addition of **2a**. Inset: intensity changes of absorbance at 550 nm. b) Fluorescent spectra (0.05 mM, $CHCl_3$: CH_3CN = 1 : 1) of **1a** (black line) and **1a**/**2a** (red line). The emergence of MMLCT absorption/emission bands support the existence of Pt---Pt metal–metal interactions for complex **1a**/**2a**. Nonlinear curve-fitting of the collected absorbance data at 550 nm provides the K_a value of (4.69 ± 0.13) × 10^4 M^{-1} for complex **1a**/**2a**.

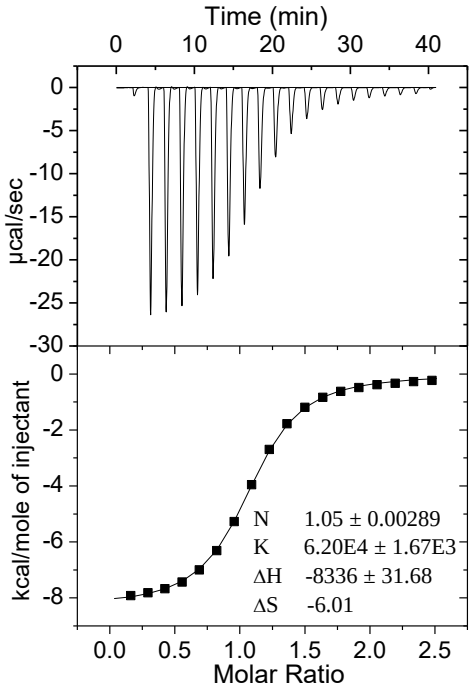

Figure S9. ITC experiments by consecutive injecting of **2a** (8.00 mM) into the solution of **1a** (0.40 mM, $CHCl_3$: CH_3CN = 1 : 1). The binding stoichiometry between **1a** and **2a** is determined to be 1 : 1, as reflected by the abrupt change in the curve. Fitting the exothermic binding isotherm data with one-site model provides the K_a value of (6.20 ± 0.17) × 10^4 M^{-1} for complex **1a**/**2a**.

*7. DFT calculation for complex **1b**/**2a***

X-ray crystallography provides the reliable structural information for non-covalent complexation systems. On this account, we tried to grow high-quality single crystals for the supramolecular tweezering complexes. Even though considerable attempts have been carried out, unfortunately it fails to get the desired crystals. As an alternative way, we turned to clarify the non-covalent complexation structures *via* density functional theory (DFT) calculations.

For the optimized geometry of **1b**/**2a** (Figure S10), triple stacking of Pt(II) atoms is validated by the short Pt---Pt distances of 3.48 and 3.53 Å. Hence, it supports the existence of Pt---Pt metal–metal interactions, which is consistent with the UV/Vis and fluorescent experimental results. Meanwhile, inter-planar distances between the alkynylplatinum(II) terpyridine and isocyanideplatinum(II) diphenylpyridine pincers are determined to be 3.63 Å. Accordingly, it can be concluded that both Pt---Pt metal–metal and donor–acceptor interactions are involved in complex **1b**/**2a**.

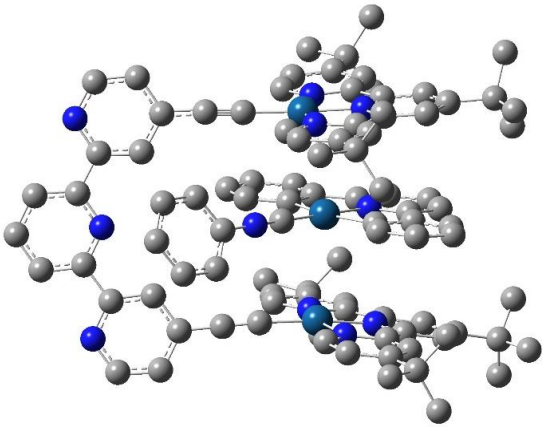

Figure S10. Optimized geometry of complex **1b**/**2a**.

8. Photosensitization capability test

$^1O_2$ generation rate (v/ min^{-1}•M^{-1}) can be calculated on the basis of the UV/Vis measurements (Figure S11a). Specifically, it is determined by the following equation,

$$v = k/c \qquad \textbf{(Eq. S2)}$$

In particular, k is the slope of the corresponding curve, while c denotes the monomer concentration.

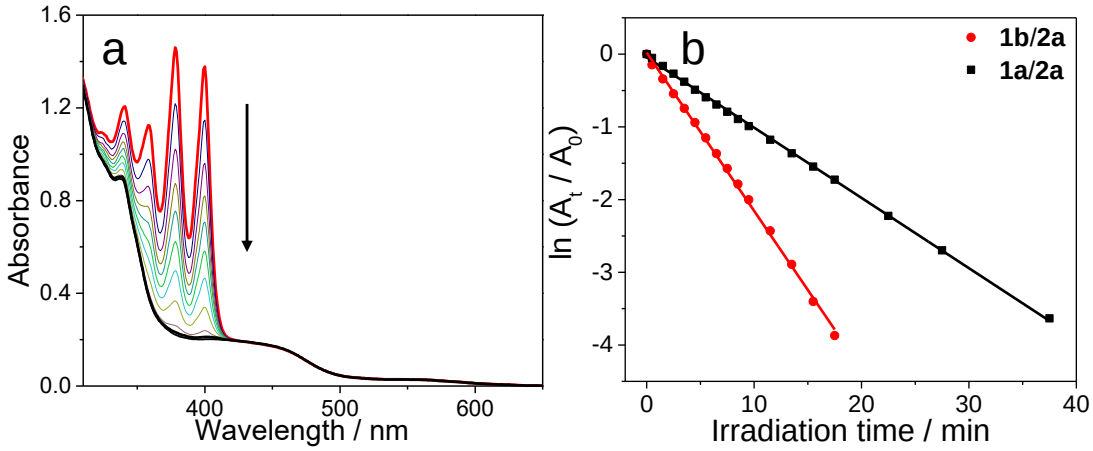

Figure S11. a) UV/Vis absorption changes of DMA (0.25 mM, $CHCl_3$: CH_3CN = 1 : 1) upon visible light irradiation (590 nm, 12 W), with the employment of complex **1b**/**2a** (c = 0.03 mM) as the photosensitizer. b) Photosensitization efficiency of complexes **1a**/**2a** (■) and **1b**/**2a** (●), by monitoring time-dependent absorbance of DMA at 401 nm. It is obvious that **1b**/**2a** displays reinforced photosensitive efficiency than that of **1a**/**2a** (725 min^{-1} M^{-1} *vs* 322 min^{-1} M^{-1}).

*9. Photo-oxidative cyanation of tertiary amine **3***

General procedure for the photo-catalytic reaction: tertiary amine **3** (0.10 mmol), TMSCN (0.15 mmol), and the corresponding photosensitizers were dissolved in 10 mL $CHCl_3/CH_3CN$ (1 : 1, *v*/*v*) in a 13 cm-tall quartz tube. The reaction mixture was bubbled with solvent-saturated oxygen gas in 20 seconds, and irradiated with a 100 W OLED lamp ($\lambda > 590$ nm) as the light source at room temperature. Upon light irradiation, the benzylic resonance H_a of **3** locating at 4.41 ppm progressively decreases. In the meantime, the newly-formed benzylic signal $H_{a'}$ locating at 5.52 ppm gradually increases (Figure S12). After irradiating for several hours, the solvent was evaporated and the product yield was calculated, by using 4,4'-dimethyl-2,2'-bipyridine as the internal ^1H NMR standard. Turnover numbers (TON) value was calculated by product yield *vs* reaction time and catalyst loading percentage.

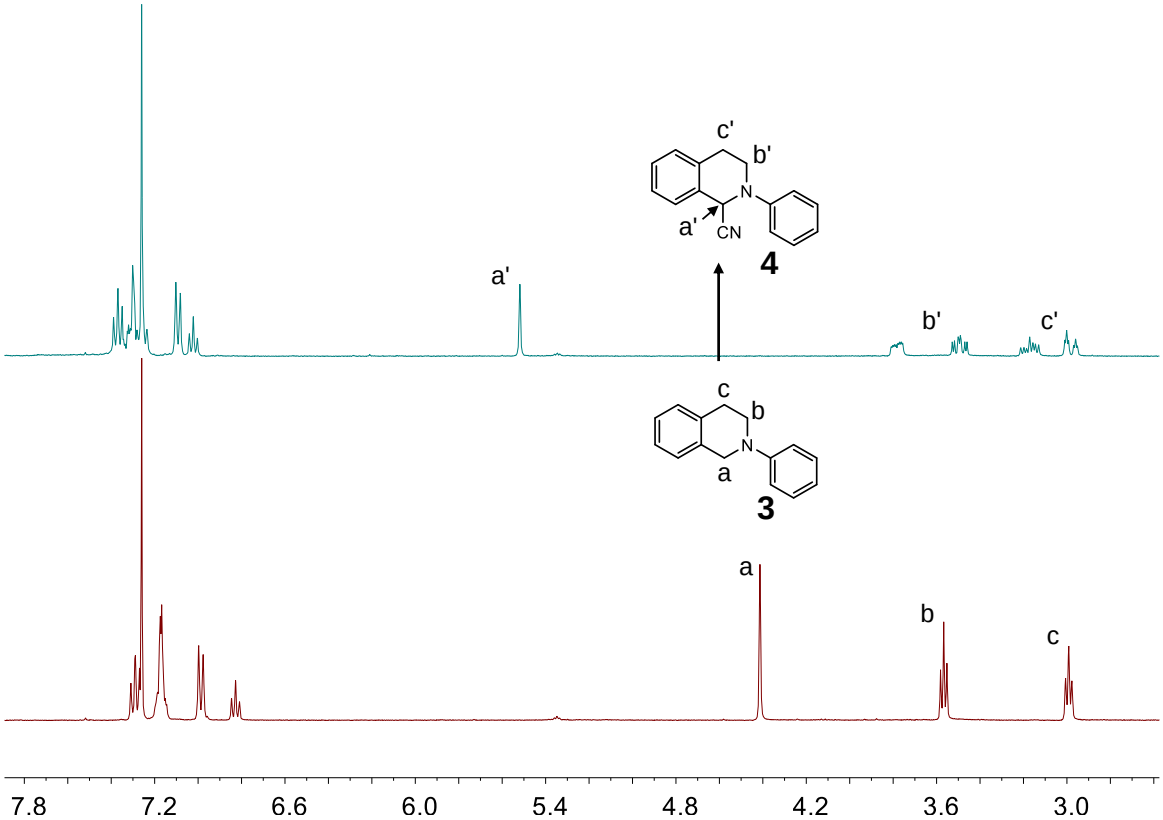

Figure S12. Photo-oxidative cyanation of tertiary amine **3** to **4**. Herein complex **1b**/**2a** was employed as the photosensitizer to illustrate the organic conversion.

*10. Photo-cleavage reaction of coumarin derivative **5***

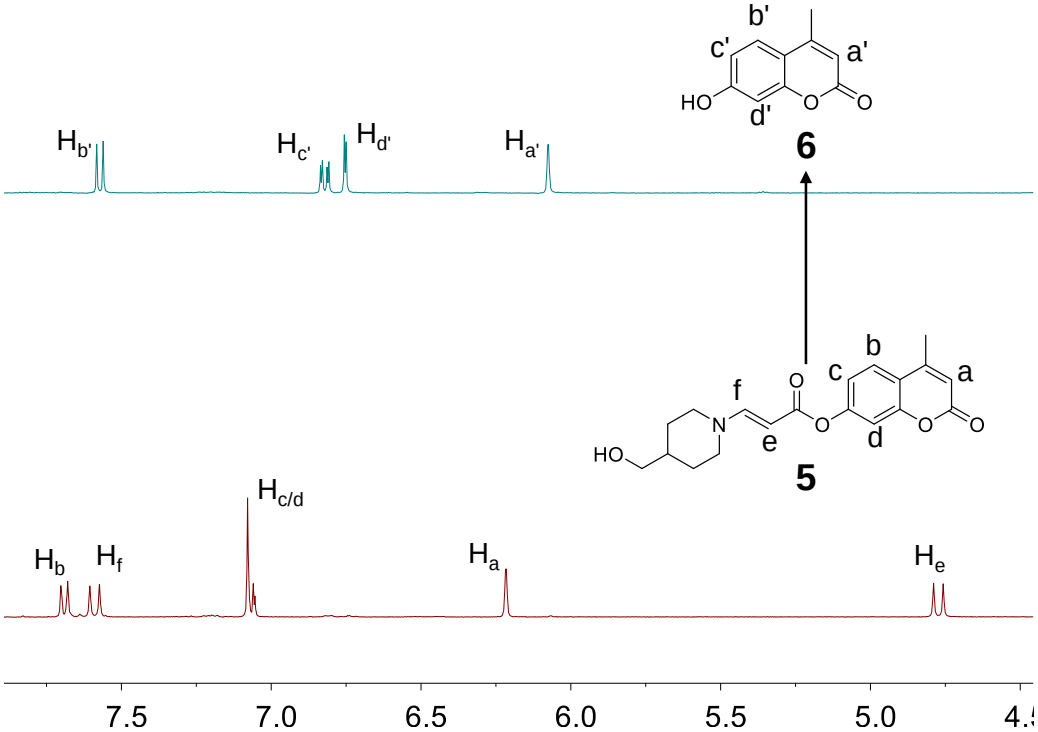

Figure S13. Photo-cleavage of coumarin derivative **5** to **6**. Conversion of **5** to **6** can be monitored by ^{1}H NMR experiments (CD_3CN : D_2O =1 : 1, complex **1b**/**2a** was employed as the photo-catalyst).

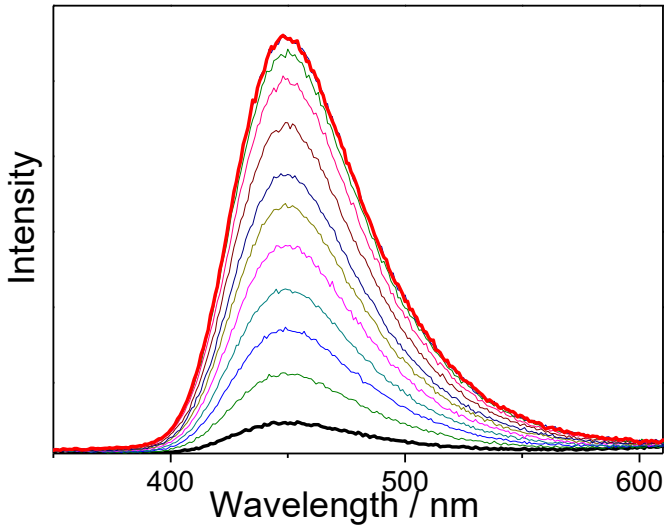

Figure S14. Photo-cleavage reaction of **5** to **6** (20 μM in 95% water/5% DMF, complex **1b**/**2a** as the photocatalyst, 590 nm, 12w), accompanying with the "turning-on" fluorescence at 450 nm.

*11. Cation-triggered responsiveness of **1b** and **1b**/**2a***

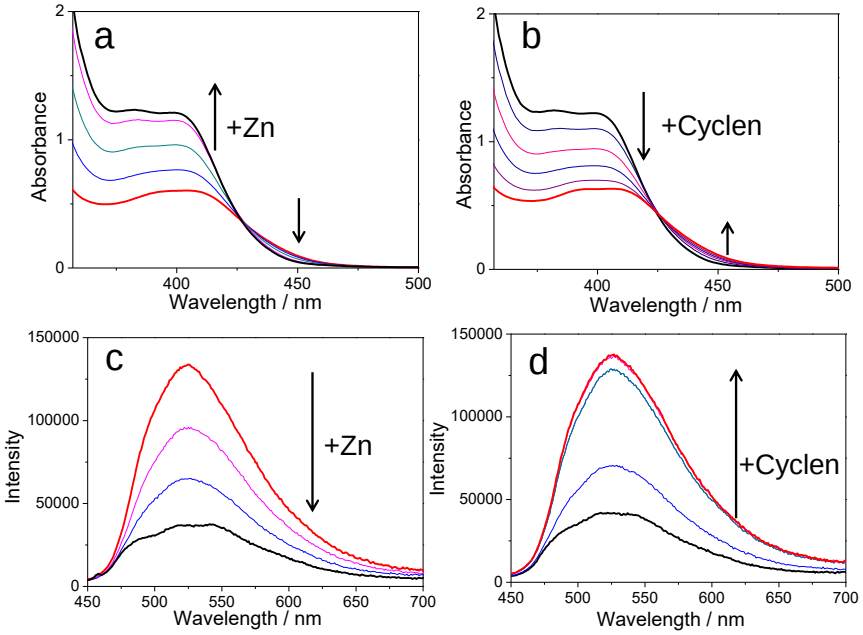

Figure S15. UV/Vis absorption spectral changes of **1b** (0.05 mM, $CHCl_3$: CH_3CN = 1 : 1) upon the successive addition of a) $Zn(OTf)_2$ and b) cyclen. Fluorescent spectral changes of **1b** (0.05 mM, $CHCl_3$: CH_3CN = 1 : 1) upon the successive addition of c) $Zn(OTf)_2$ and d) cyclen. The addition of Zn^{2+} ion leads to the blue-shifting of MLCT/LLCT absorption band, as well as the decline of fluorescent intensity. Such phenoma suggest the "*U*"- to "*W*"-shaped conformational transition of **1b**. The absorption and fluorescent spectra completely restore after the successive addition of cyclen as the competitive ligand.

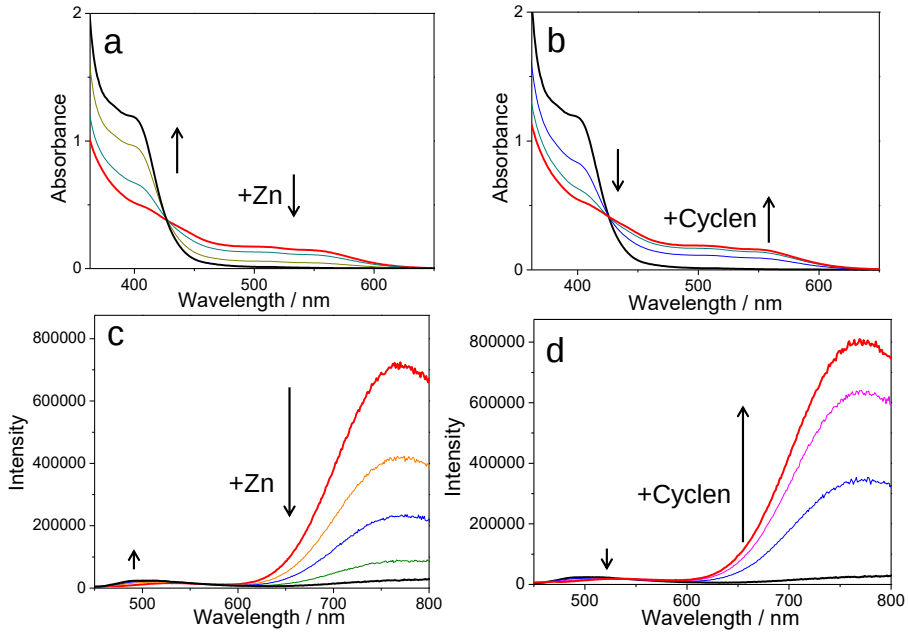

Figure S16. UV/Vis absorption spectral changes of **1b**/**2a** (0.05 mM, $CHCl_3$: CH_3CN = 1 : 1) upon the successive addition of a) $Zn(OTf)_2$ and b) cyclen. Fluorescent spectral changes of **1b**/**2a** (0.05 mM, $CHCl_3$: CH_3CN = 1 : 1) upon the successive addition of c) $Zn(OTf)_2$ and d) cyclen. The addition of Zn^{2+} ion leads to the vanish of MMLCT absorbance and emission band, suggesting the disruption of complex **1b**/**2a**. The MMLCT absorption and fluorescent spectra completely restore after the successive addition of cyclen.

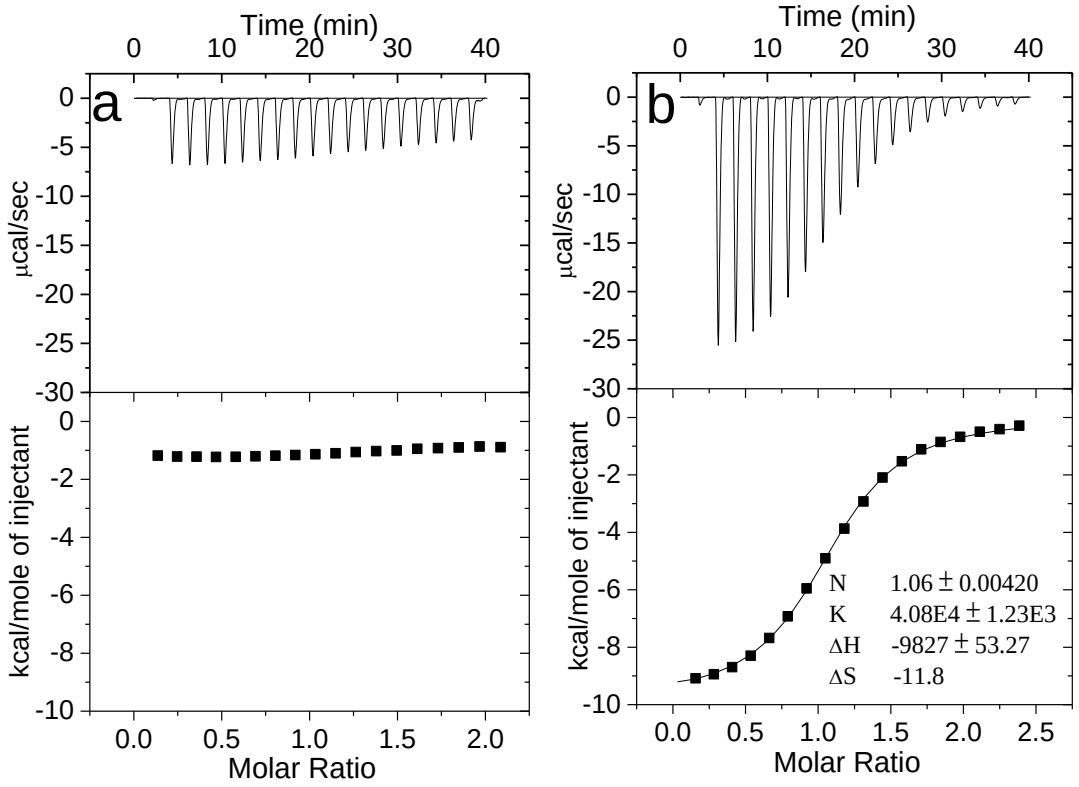

Figure S17. ITC experiments by consecutive injecting of **2a** (8.00 mM) into the solution of a) **1b** + Zn^{2+} (0.40 mM, $CHCl_3$: CH_3CN = 1 : 1), and b) **1a** + Zn^{2+} (0.40 mM, $CHCl_3$: CH_3CN = 1 : 1). Notably, negligible heat exchange occurs when titrating **2a** into the mixture solution of **1b** and Zn^{2+}. Such phenomena suggest that **1b** undergoes "U"- to "W"-shaped conformational transition upon adding Zn^{2+} ion, which influences non-covalent binding capability toward the complemenatry guest **2a**. In stark contrast, the presence of Zn^{2+} ion hardly affects the non-covalent binding affinity between **1a** and **2a** (with Zn^{2+} ion, K_a = (4.08 ± 0.12) × 10^4 M^{-1} for **1a**/**2a**; without Zn^{2+} ion, K_a = (6.20 ± 0.17) × 10^4 M^{-1} for **1a**/**2a**, see Figure S9), validating the importance of dynamic switching elements for the stimuli-responsive molecular tweezer/guest complexation behaviors.

*12. "On-demand" photo-catalytic efficiency of **1b**/**2a***

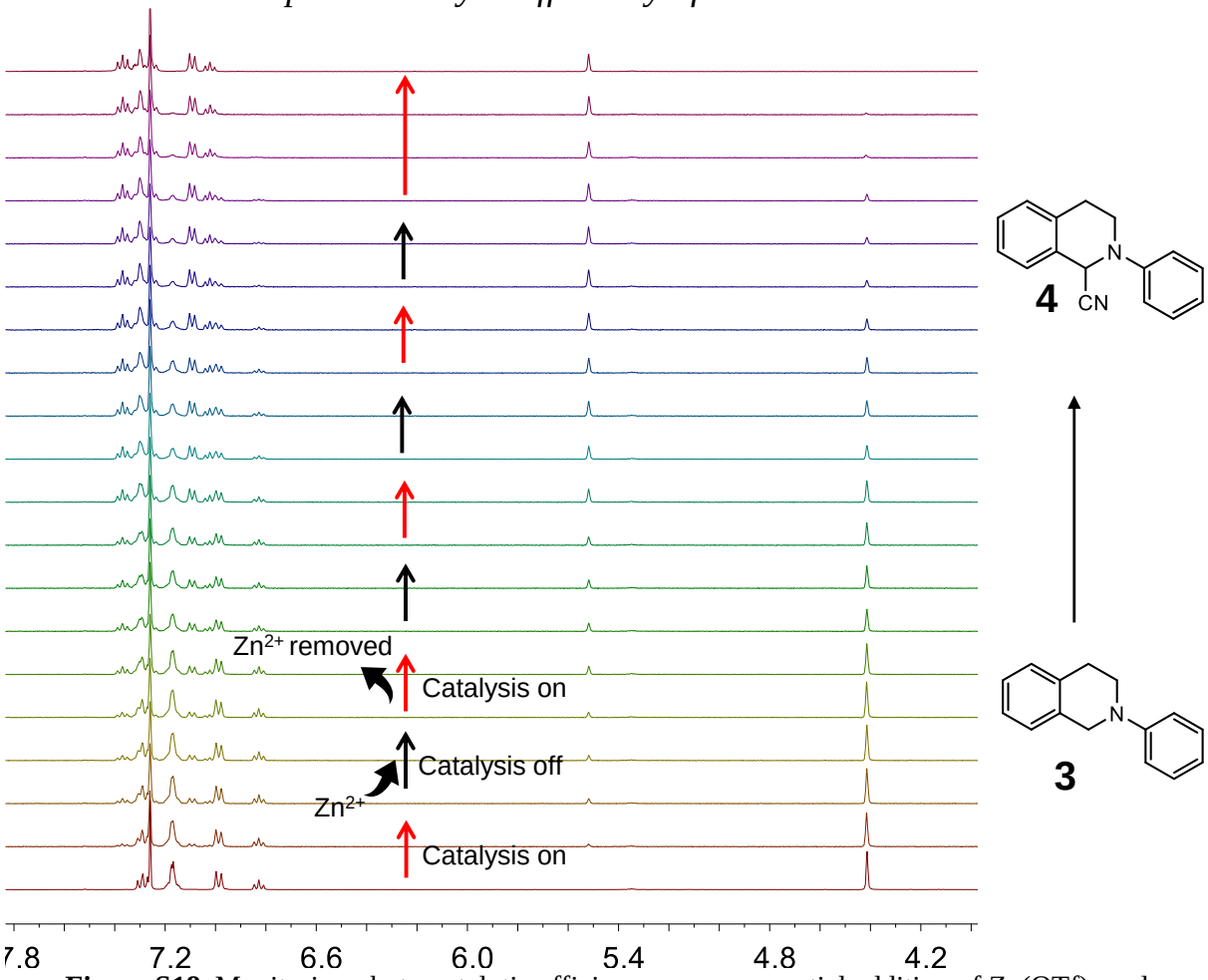

Figure S18. Monitoring photo-catalytic efficiency upon sequential addition of $Zn(OTf)_2$ and terpyridine (as the competitive ligand) to complex **1b**/**2a** (0.2% equivalent to **3**). Depending on ^1H NMR measurements, "on-demand" photo-oxidative cyanation of tertiary amine **3** can be achieved, by manipulating the revival and loss of photosensitization capability of **1b**/**2a**.

*13. Synthesis of **1b***

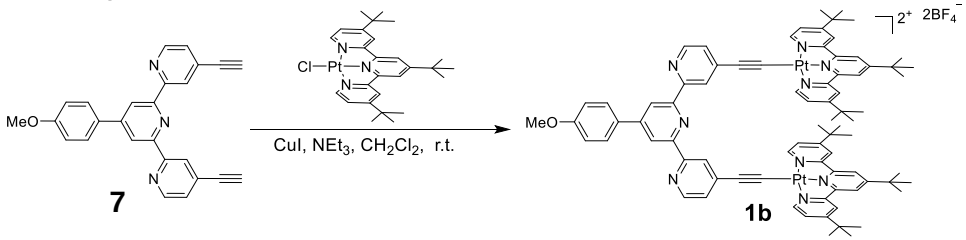

Scheme S1. Synthetic route to molecular tweezer **1b**.

Compound **7** (0.13 g, 0.32 mmol), [Pt(tpy)Cl](BF$_4$) (0.58 g, 0.80 mmol), CuI (0.02 g, 0.32 mmol) and NEt$_3$ (4 mL) in CH_2Cl_2 (60 mL) were stirred at room temperature for 48 hours. The mixture was evaporated under reduced pressure, and the residue was purified by column chromatography (alumina, CH_3OH/CH_2Cl_2, 1: 100 *v*/*v* as the eluent) to afford **1b** as an orange solid (0.51 g, 91%). ^{1}H NMR (300 MHz, $CDCl_3$) δ (ppm): 9.32 (s, 2H), 7.99 (d, J = 6.2 Hz, 8H), 7.89 (s, 4H), 7.47 (d, J = 4.9 Hz, 2H), 7.06 (s, 2H), 6.83 (dd, J = 6.0, 1.8 Hz, 4H), 6.76 (d, J = 3.4 Hz, 4H), 6.66 (d, J = 4.5 Hz, 2H), 3.73 (s, 3H), 1.22 (s, 36H), 1.11 (s, 18H). ^{13}C NMR (75 MHz, DMSO-d_6) δ (ppm): 166.4, 165.0, 160.5, 157.3, 154.2, 153.7, 153.1, 152.7, 147.6, 146.4, 135.0, 128.9, 127.0, 124.9, 122.9, 120.9, 115.1, 107.1, 100.6, 67.0, 55.6, 52.0, 36.8, 36.0, 29.9, 29.6. ESI–MS *m*/*z*: $[M - 2BF_4]^{2+}$, calcd for $C_{80}H_{85}N_9OPt_2$, 788.8087; found, 788.8057; error, 3.8 ppm.

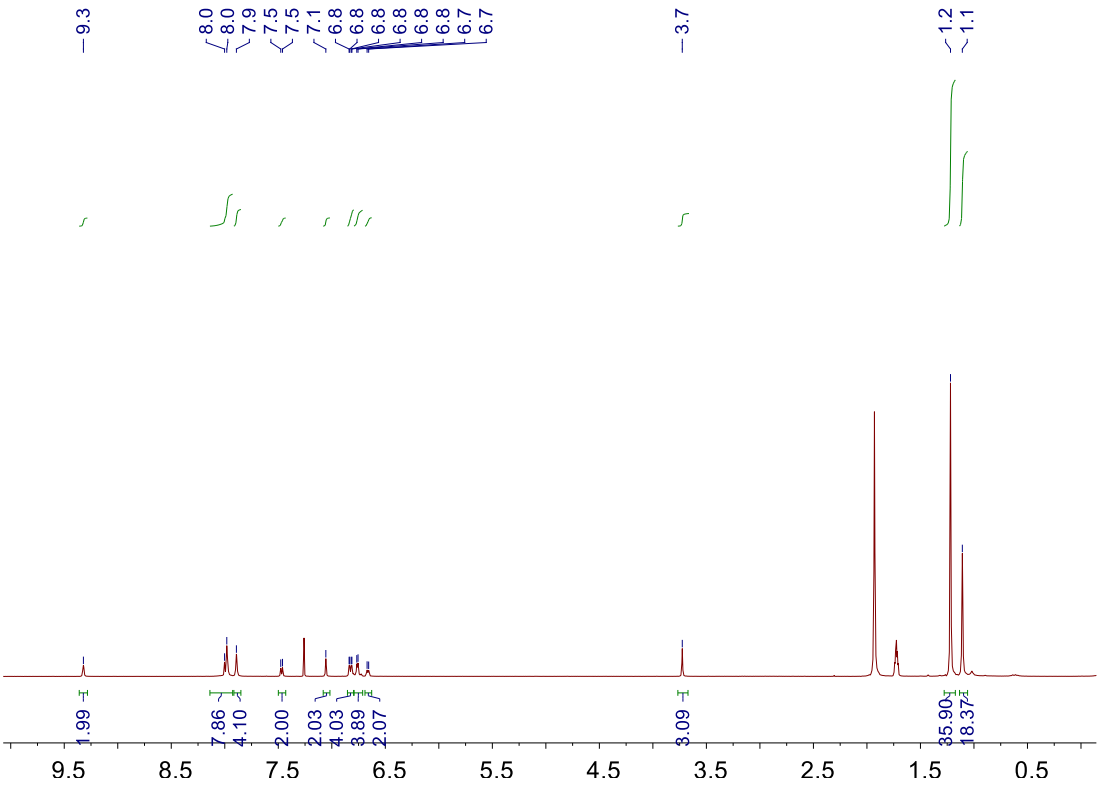

Figure S19. ^{1}H NMR spectrum (300 MHz, $CDCl_3$, room temperature) of **1b**.

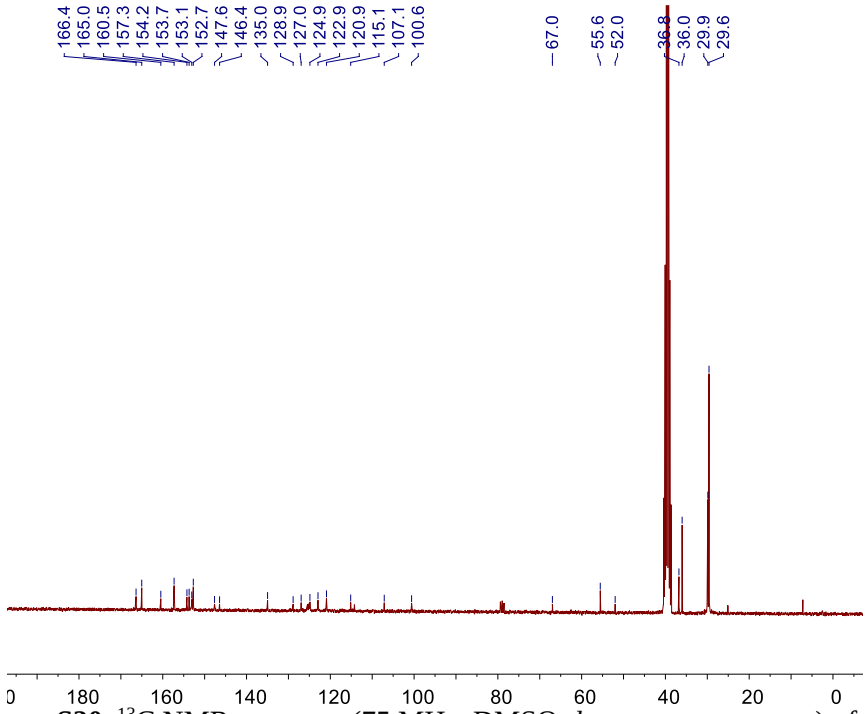

Figure S20. ^{13}C NMR spectrum (75 MHz, DMSO-d_6, room temperature) of **1b**.

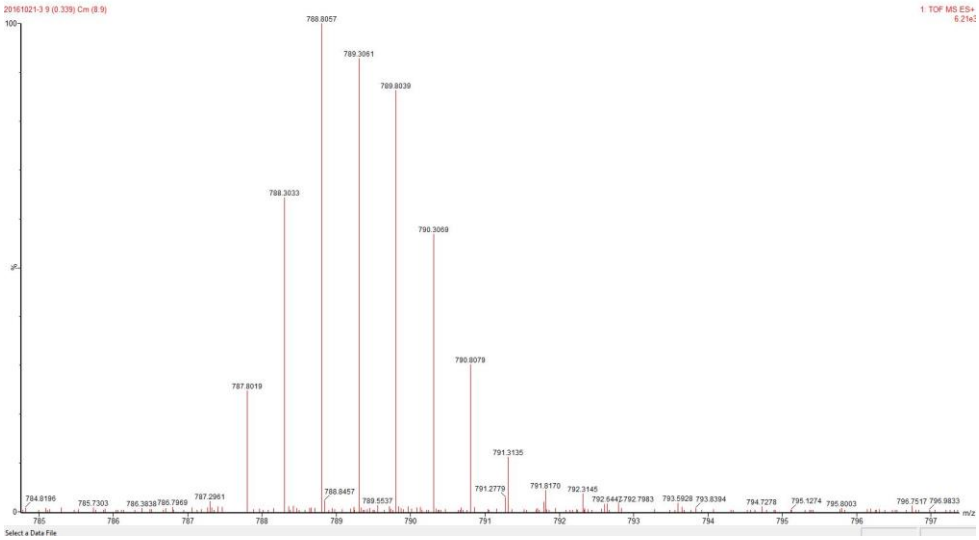

Figure S21. Electrospray ionization spectrum of **1b**.

References:

[S1] Y. Tanaka, K. M. -C. Wong and V. W. -W. Yam, *Chem. Sci.* 2012, **3**, 1185.

[S2] Y.-K. Tian, Y.-G. Shi, Z.-S. Yang and F. Wang, *Angew. Chem. Int. Ed.* 2014, **53**, 6090.

[S3] Z.-J. Li, Y.-F. Han, F. Jin, Z.-C. Gao, Z. Gao, L. Ao and F. Wang, *Dalton Trans.* 2016, **45**, 17290.

[S4] Z.-J. Li, Y.-F. Han, Z.-C. Gao and F. Wang, *ACS Catal.* 2017, **7**, 4676.

[S5] Gaussian 09, Revision D.01, M. J. Frisch, G. W. Trucks, H. B. Schlegel, G. E. Scuseria, M. A. Robb, J. R. Cheeseman, G. Scalmani, V. Barone, B. Mennucci, G. A. Petersson, H. Nakatsuji, M. Caricato, X. Li, H. P. Hratchian, A. F. Izmaylov, J. Bloino, G. Zheng, J. L. Sonnenberg, M. Hada, M. Ehara, K. Toyota, R. Fukuda, J. Hasegawa, M. Ishida, T. Nakajima, Y. Honda, O. Kitao, H. Nakai, T. Vreven, J. A. Montgomery, Jr., J. E. Peralta, F. Ogliaro, M. Bearpark, J. J. Heyd, E. Brothers, K. N. Kudin, V. N. Staroverov, T. Keith, R. Kobayashi, J. Normand, K. Raghavachari, A. Rendell, J. C. Burant, S. S. Iyengar, J. Tomasi, M. Cossi, N. Rega, J. M. Millam, M. Klene, J. E. Knox, J. B. Cross, V. Bakken, C. Adamo, J. Jaramillo, R. Gomperts, R. E. Stratmann, O. Yazyev, A. J. Austin, R. Cammi, C. Pomelli, J. W. Ochterski, R. L. Martin, K. Morokuma, V. G. Zakrzewski, G. A. Voth, P. Salvador, J. J. Dannenberg, S. Dapprich, A. D. Daniels, O. Farkas, J. B. Foresman, J. V. Ortiz, J. Cioslowski, and D. J. Fox, Gaussian, Inc., Wallingford CT, 2013.

[S6] DFT calculations were performed under B3LYP/6-31G(d) level by virtue of Gaussian 09, A.02 revision. Gaussian 09, Revision A.02, M. J. Frisch, G. W. Trucks, H. B. Schlegel, G. E. Scuseria, M. A. Robb, J. R. Cheeseman, G. Scalmani, V. Barone, B. Mennucci, G. A. Petersson, H. Nakatsuji, M. Caricato, X. Li, H. P. Hratchian, A. F. Izmaylov, J. Bloino, G. Zheng, J. L. Sonnenberg, M. Hada, M. Ehara, K. Toyota, R. Fukuda, J. Hasegawa, M. Ishida, T. Nakajima, Y. Honda, O. Kitao, H. Nakai, T. Vreven, J. A. Montgomery, Jr., J. E. Peralta, F. Ogliaro, M. Bearpark, J. J. Heyd, E. Brothers, K. N. Kudin, V. N. Staroverov, R. Kobayashi, J. Normand, K. Raghavachari, A. Rendell, J. C. Burant, S. S. Iyengar, J. Tomasi, M. Cossi, N. Rega, J. M. Millam, M. Klene, J. E. Knox, J. B. Cross, V. Bakken, C. Adamo, J. Jaramillo, R. Gomperts, R. E. Stratmann, O. Yazyev, A. J. Austin, R. Cammi, C. Pomelli, J. W. Ochterski, R. L. Martin, K. Morokuma, V. G. Zakrzewski, G. A. Voth, P. Salvador, J. J. Dannenberg, S. Dapprich, A. D. Daniels, O. Farkas, J. B. Foresman, J. V. Ortiz, J. Cioslowski, and D. J. Fox, Gaussian, Inc., Wallingford CT, 2009.

[S7] B. Doistau, A. Tron, S. A. Denisov, G. Jonusauskas, N. D. McClenaghan, G. Gontard, V. Marvaud, B. Hasenknopf and G. Vives, *Chem.–Eur. J.* 2014, **20**, 15799.